Bull. Mater. Sci., Vol. 34, No. 7, December 2011, pp. 1313–1317. © Indian Academy of Sciences.

Solvothermal synthesis and characterization of acicular α-Fe_2O_3 nanoparticles

S BASAVARAJA[†], D S BALAJI, MAHESH D BEDRE, D RAGHUNANDAN[††], P M PRITHVIRAJ SWAMY and A VENKATARAMAN*

Materials Chemistry Laboratory, Department of Materials Science, Gulbarga University, Gulbarga 585 106, India
[†]Present address: Veeco-India Nanotechnology Laboratory,
Jawaharlal Nehru Centre for Advanced Scientific Research, Jakkur, Bangalore 560 064, India
[††]H.K.E.S. College of Pharmacy, Sedam Road, Gulbarga 585 101, India

MS received 14 April 2010

Abstract. **Nanometer-sized α-Fe_2O_3 particles have been prepared by a simple solvothermal method using ferric acetylacetonate as a precursor. The products were characterized by X-ray diffraction (XRD), energy dispersive X-ray microanalysis (EDAX), X-ray photoelectron spectroscopy (XPS), scanning electron microscopy (SEM), transition electron microscopy (TEM), infrared spectroscopy (IR) and thermal analysis (TG–DTA). XRD indicates that the product is single-phase α-Fe_2O_3 with rhombohedral structure. Bundles of acicular shaped nanoparticles are seen in TEM images with an aspect ratio ~ 12; typically 8–12 nm wide and over 150 nm long. The α-Fe_2O_3 nanoparticles posses a high thermal stability, as observed on thermal analysis traces.**

Keywords. **α-Fe_2O_3; solvothermal; transmission electron microscope; X-ray diffraction.**

1. Introduction

There is great interest in the preparation of transition metal oxide nanoparticles as a result of their finding of extensive use in high-performance ceramics (Siegal 1996), as media for magnetic data storage (Matijevic 1993), in catalysis (White *et al* 1997), for solar energy conversion (Cherepy *et al* 1998) and in the preparation of ferrofluids (Kang *et al* 1996). Among these materials, α-Fe_2O_3 has been extensively studied due to its wide technological applications in catalysis, pigments, recording medium, sensors and electrode materials (Faust *et al* 1989; Cornell and Schwertmann 1996; Han *et al* 2001; Chen *et al* 2005) because of its low cost, high resistance to corrosion and environmental friendly properties. Although α-Fe_2O_3 nanoparticles have been produced through different synthetic routes (Niederberger *et al* 2002; Chen *et al* 2005; Wen *et al* 2005), it was observed that the nanoparticles manifested very different physical and chemical properties depending on their microstructure, such as size uniformity and crystallinity. Therefore, developing a synthesis method that can maintain size uniformity and crystallinity is critical for the application of these nanoparticles (Lu *et al* 1999).

There are several methods for synthesizing nanosized ceramic materials, such as, hydrothermal, co-precipitation, combustion, sol–gel, precursor, spray drying and freeze drying, microemulsion and reverse micelle method and microwave techniques (Suresh *et al* 1991; Awschalom and Vincenzo 1995; Pileni and Moumen 1996; Yu and Gadalla 1996; Dawson 1998; Maclaren and Ponton 1998; Albuquerque *et al* 1999; Chen *et al* 1999; Gajbhiye *et al* 1999; Liu *et al* 2000; Basavaraja *et al* 2007; Lagashetty *et al* 2007). Among these methods, the hydrothermal synthesis, which is one of the soft solution routes, is of current interest and is attractive and a promising method to obtain nanocrsytalline metal oxide particles. The hydrothermal process, in which the chemical reaction could take place under auto-generated pressure upon heating between the temperature of boiling and critical points of water (100–374°C), is efficient to achieve the crystalline phase at relatively low temperatures (Komarneni *et al* 1988). The hydrothermal process proceeds with aqueous and/or non-aqueous systems as the reaction medium and is environmental friendly since the reactions are carried out in a closed system. The phase, particle size and crystallinity can easily be controlled by hydrothermal conditions (Kolen'ko *et al* 2004). In particular, the particles prepared through hydrothermal synthesis are expected to have uniform-sized large surface area, smaller crystallite size and higher stability than those obtained by other methods. This technique is also called solvothermal by many researchers (Dow and Schuller 1987), while in the special case of the solvent being water, often called hydrothermal.

*Author for correspondence (raman_chem@rediffmail.com)

Recently, iron oxide nanoparticles of different phases were successfully prepared by this technique (Li *et al* 2002; Hou *et al* 2003; Titirici *et al* 2006; Zheng *et al* 2006). Hou *et al* (2003) have synthesized magnetite (Fe_3O_4) nanoparticles using ferric acetylacetonate through a solvothermal reduction approach in the presence of surfactants/stabilizers. Herein, we report, almost uniform-sized acicular-shaped α-Fe_2O_3 nanoparticles have been synthesized by solvothermal decomposition of ferric acetylacetonate in toluene at 160°C without using any surfactants/stabilizers. The use of this precursor is that the thermal behaviour is well studied by many authors (Pal and Sharon 2000; Mallikarjuna *et al* 2003) and it easily produces iron oxide of different phases by combustion (Pal and Sharon 2000; Mallikarjuna *et al* 2003). The as synthesized α-Fe_2O_3 nanoparticles were characterized for their structure, morphology, bonding and thermal properties.

2. Experimental

Ferrous ammonium sulphate, toluene, ammonia, ethanol and hydrogen peroxide were of AR grade and were used as received without further purification. Ferric acetylacetonate was prepared by reported procedure (Singh and Kushawaha 2000).

In a typical experiment, the α-Fe_2O_3 nanoparticles were prepared by dissolving 80 mg of ferric acetylacetonate complex in a 30 ml of toluene. To this a few drops of hydrogen peroxide was added under vigorous stirring to facilitate the decomposition of ferric acetylacetonate to oxide under the experimental conditions. The resultant mixture was then placed in a 45 ml Teflon-liner hydrothermal bomb (corresponding to 70% filling of the bomb). The sealed bomb was placed in an autoclave, which was heated to 160°C for 8 h. During the thermal treatment the metal complex got decomposed by the thermal energy in the solvent. After the reaction was completed, the autoclave was allowed to cool to room temperature naturally. The resultant brown solid product was filtered, washed several times with distilled water and absolute ethanol to remove impurities, and then dried at 60°C in air. The obtained brown powder was collected for the structural, morphological and thermal characterization.

The XRD pattern was obtained employing a GEOL JDX-8p spectrometer using CuKα radiation (λ = 1·54 Å). The X-ray generator was operated at 30 kV and 20 mA. The scanning range, 2θ was selected. The scanning speed of 1°/min and a chart speed of 20 mm/min were used for the precise determination of the lattice parameters. XPS (Physical Electronics PHI-5600, Russia) measurements were made with an Al Kα X-ray source (1253·6 eV). The morphology and elemental composition of the nanoparticles were characterized using coupling JSM-840A scanning electron microscope. The electron microscope was operated at 20 kV. The sample was made conducting by the sputtering of gold using a Poloron DC 'sputtering unit' operated at 1·4 kV and 18–20 mA. Sample for TEM was prepared by placing a drop of the ethanol suspension of the nanoparticles on carbon-coated Cu TEM grids and subsequently drawing off excess solvent. The grids were examined using a Philips CM 200 operating at 200 kV. The FT–IR spectrum of α-Fe_2O_3 nanoparticles was recorded on a Perkin–Elmer Spectrum One in the range 4000–400 cm^{-1} at resolution of 4 cm^{-1} by making KBr pellets. Simultaneous TG–DTA was obtained from Mettlar Teledo Star instruments (Weinheim, Germany) under a dynamic flow of nitrogen at a flow rate of 100 ml/min and at a heating rate of 10°C/min.

3. Results and discussion

The phase and purity of the as synthesized product was examined by X-ray diffraction (XRD) pattern. The XRD of the α-Fe_2O_3 nanoparticles is shown in figure 1. All these peaks were successfully assigned and indexed in the figure considering a rhombohedral unit cell of standard JCPDS file no. 24-72 having lattice constant a = 5·038 Å and c = 13·772 Å with space group $R\,\bar{3}c$ (148). No other phase was detected in the XRD pattern indicating the high purity of the final product.

The mean particle diameter was calculated from the XRD pattern according to the line width of the (104) plane refraction peak using the following Debye–Scherrer equation (Cornell and Schwertmann 1996):

$$D = \frac{K\lambda}{\beta_{1/2}\cos\theta}.$$

The equation uses the reference peak width at angle θ, where λ is the X-ray wavelength (1·5418 Å) and $\beta_{1/2}$ is the shape factor, about 0·9 for iron oxides. The average crystallite size calculated from peak width is about 16 nm, which is in accordance with the TEM results discussed later.

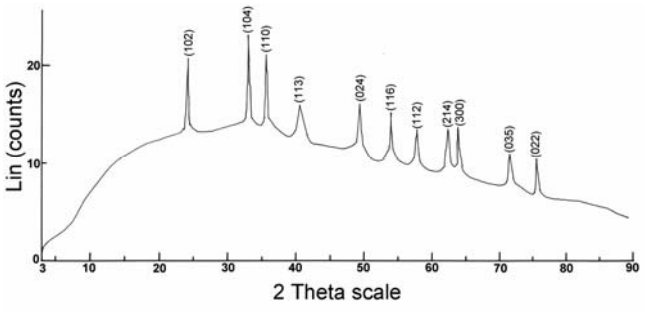

Figure 1. XRD pattern of as synthesized α-Fe_2O_3 nanoparticles.

The presence of the metal and impurities in the α-Fe_2O_3 nanoparticles were examined by energy dispersive microanalysis of X-ray (EDAX) studies. The EDAX spectrum of as synthesized α-Fe_2O_3 is shown in figure 2. This figure shows the presence of the only Fe and O with no impurity signal.

Figure 3 shows the X-ray photoelectron spectroscopy (XPS) spectra of α-Fe_2O_3 sample. XPS (figure 3a) shows the Fe $2p_{3/2}$ peak at 711·0 eV. C 1s peak of the carbon contamination over the sample is referenced at 284·6 eV. Shake up satellite ~ 8 eV above the Fe $2p_{1/2}$ and Fe $2p_{3/2}$ peaks are visible. Separation of the 2*p* doublet is ~ 13·6 eV. All these features are typical of Fe_2O_3. The peak maximum for α and γ are reported to be at the same position (711·0 eV) but the structure near the maximum in the peak is different (McIntyre and Zetaruk 1977). Gupta and Sen (1974) calculated the multiplet structure of core *p*-level of free Fe^{3+} ion. The measured splitting of the two most intense components of the α-Fe_2O_3 Fe $2p_{3/2}$ line is 1·2 eV (McIntyre and Zetaruk 1977), as compared with 1·6 eV calculated for Fe^{3+} (Gupta and Sen 1974; McIntyre and Zetaruk 1977). The mean binding energy of ~ 711·0 eV is the same for α- and γ-Fe_2O_3. The only change is in the multiplet splitting distribution within each peak. We have observed a double peak separated by ~ 1·2 eV in Fe $2p_{3/2}$ peak. Based on this observation we presume that the peak structure corresponds to α-Fe_2O_3. The O 1s peak at 529·4 eV corresponds to O^{2-} of Fe_2O_3 and the tail at higher binding energy to hydroxyl (532·0 eV) and carboxyl formed on the sample surface (figure 3b). The Fe 3*p* peak appears at 55·4 eV (figure 3c), which is consistent with the reported values for α-Fe_2O_3 (McIntyre and Zetaruk 1977).

Figure 4 shows the typical bright field TEM image of the as synthesized α-Fe_2O_3 nanoparticles. The TEM image shows the acicular-shaped nanoparticles. These acicular-shaped nanoparticles are joined together to form bundles of aggregates. These bundles of acicular particles are separated from each other throughout the image. The widths of the acicular-shaped particles are from 8 to 12 nm and lengths are from as low as 20 nm to as high as 150 nm in size.

The corresponding selected area electron diffraction (SAED) pattern of the α-Fe_2O_3 nanoparticles is shown in

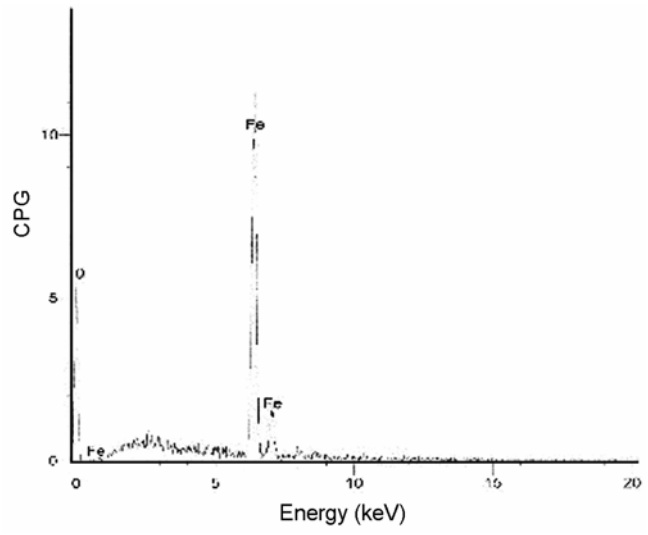

Figure 2. EDAX of the as synthesized α-Fe_2O_3 nanoparticles.

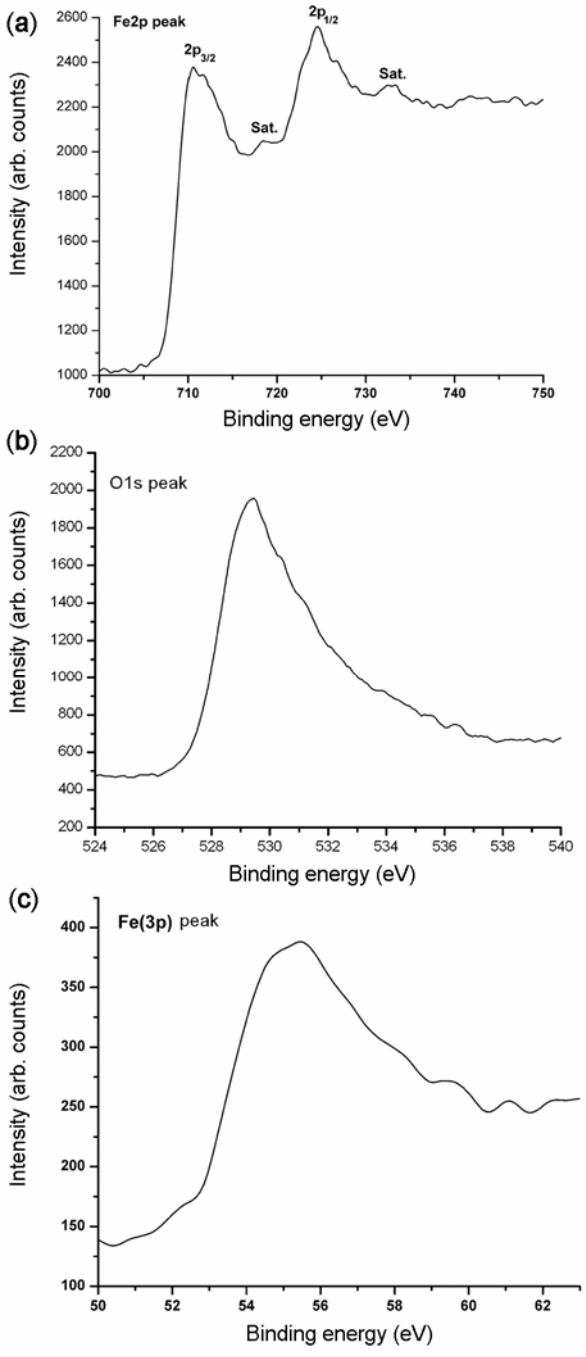

Figure 3. Major core line XPS spectrum of α-Fe_2O_3 nanoparticles. (**a**) Fe 2*p*, (**b**) O 1*s* and (**c**) Fe 3*p* spectrum.

inset of figure 4. The ED pattern consists of concentric rings along with spots over the rings. This feature indicates the polycrystallinity of the sample (Pawaskar *et al* 2002).

Fourier transform infrared (FT–IR) studies were performed to ascertain the metal–oxygen bonding. The FT–IR spectrum of as synthesized α-Fe_2O_3 sample is shown in figure 5. The α-Fe_2O_3 shows the absorption in the region 3361, 1640, 593 and 478 cm^{-1}. The peaks at 593 and 478 cm^{-1} correspond to the metal–oxygen vibrational modes. The metal–oxygen frequencies observed for α-Fe_2O_3 nanoparticles are in accordance with literature values (Gadsden 1975). The peak at 3361 and 1640 cm^{-1} corresponds to water of hydration (Rao 1963). This was further supported by the weight loss measurements of thermogravimetric analysis.

Figure 6 shows the TG–DTA traces of the as synthesized α-Fe_2O_3. The TG shows a sudden weight loss of about 3% at temperature 55°C and is due to the buoyancy effect. No further weight loss is observed up to 250°C, which indicates the thermal stability of the sample. On further heating, a loss of ~1·5% is observed over the temperature range from 250°C to 410°C. This may be due to the dehydration of the lattice hydroxyl groups strongly bound to the hematite nanoparticles (Li *et al* 2002), as is evident from the OH bands in the IR spectrum. This loss is minimal and therefore the intensity of the OH band in IR spectrum is weak. The DTA trace in figure 6 shows the small exothermic peak around 350°C, which is assigned to the dehydration of the lattice hydroxyl groups. No further weight loss is observed upon heating further to 800°C, which indicates the stability of the dehydrated iron oxide sample above 350°C. This higher thermal stability may be due to the effect of the crystallization pathways, which leads to information concerning structural defects. In addition, the amount and the microstructure of the defects also played an important role in the thermal stability of the inorganic materials (Matsumoto 2003). The lesser the defect in the structure, the higher the thermal stability of the crystal.

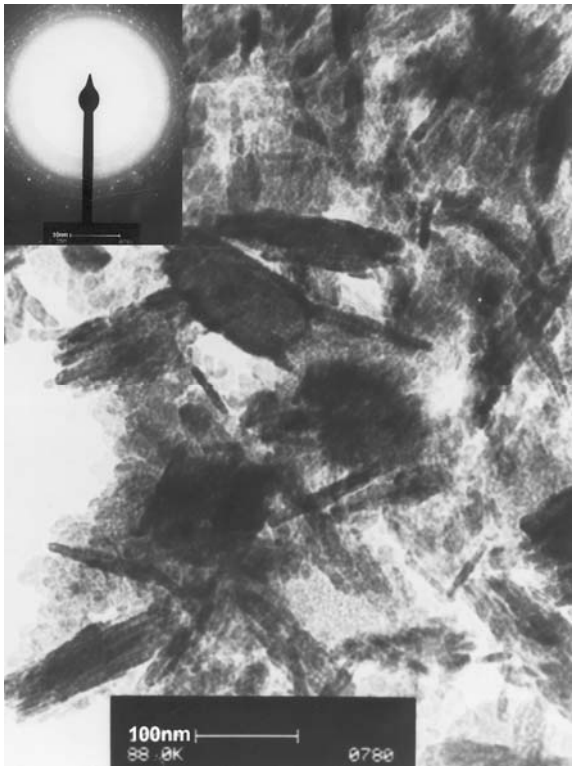

Figure 4. TEM image of the as synthesized α-Fe_2O_3 nanoparticles and inset shows the ED of the α-Fe_2O_3 nanoparticles.

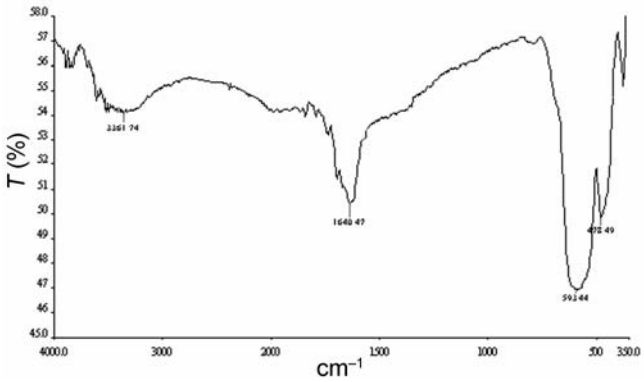

Figure 5. FT–IR spectra of the as synthesized α-Fe_2O_3 nanoparticles.

4. Conclusions

In the present work, we prepared one of the widely used ceramic material, i.e. nanosized α-Fe_2O_3, using cost-effective and relatively simple low-temperature hydrothermal synthesis. The XRD, XPS and TEM results confirm the nanocrystalline nature of the synthesized α-Fe_2O_3 particles. The detailed studies of control of

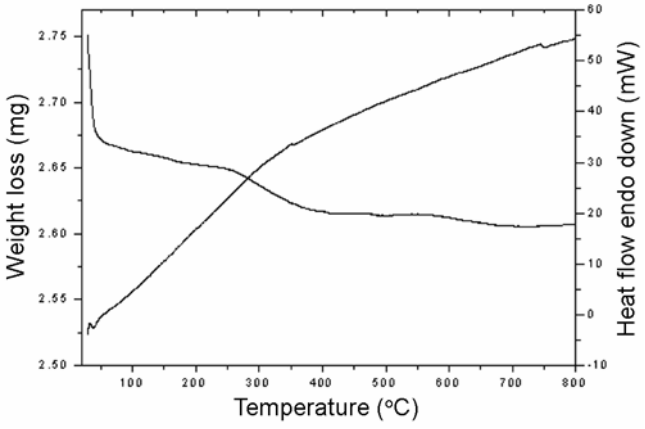

Figure 6. TG/DTA traces of the as synthesized α-Fe_2O_3 nanoparticles.

particle size and shape by controlling the reaction parameters are under way. The acicular-shaped α-Fe_2O_3 nanoparticles show applications in the areas of nanoelectronics, sensors, batteries and photocatalysis.

Acknowledgements

One of the authors (BS) acknowledges the University Grants Commission (UGC), New Delhi for financial assistance. The authors are also wish to thank Department of Science and Technology (DST), New Delhi, and University Grants Commission (Innovative Programme in Materials Chemistry), New Delhi, for financial assistance.

References

Albuquerque A S, Ardisson J D and Macedo W A A 1999 *J. Magn. Magn. Mater.* **192** 277

Awschalom D D and Vincenzo D P D 1995 *Phys. Today* **48** 43

Basavaraja S, Vijayanand H, Venkataraman A, Deshpande U P and Shripathi T 2007 *Synth. React. Inorg. Met.-Org. Nano-Met. Chem.* **37** 409

Chen J, Xu L, Li W and Gou X 2005 *Adv. Mater.* **17** 582

Chen Q, Rondinone A J, Chakoumakos B C and Zhang Z J 1999 *J. Magn. Magn. Mater.* **194** 1

Cherepy N J, Liston D B, Lovejoy J A, Deng H and Zhang J Z 1998 *J. Phys. Chem.* **B102** 770

Cornell R M and Schwertmann U 1996 *The iron oxides: structure, properties, reactions, occurrence and uses* (VCH: Weinheim)

Dawson W J 1988 *Am. Ceram. Soc. Bull.* **67** 1673

Dow J D and Schuller I K 1987 *Interfaces, superlattices, and thin films; materials research society symposia proceeding* (Pittsburgh: Materials Research Society) **Vol. 77**

Faust B C, Hoffmann M R and Bahnemann D W 1989 *J. Phys. Chem.* **93** 6371

Gadsden J A 1975 *Infrared spectra of minerals and related inorganic compounds* (England: Butterworths Publications)

Gajbhiye N S, Prasad S and Balaji G 1999 *IEEE Trans. Magn.* **35** 2155

Gupta R P and Sen S K 1974 *Phys. Rev.* **B10** 71

Han J S, Bredow T, Davey D E, Yu A B and Mulcahy D E 2001 *Sens. Actuators* **B75** 18

Hou Y, Yu J and Gao S 2003 *J. Mater. Chem.* **13** 1983

Kang Y S, Risbud S, Ranbolt J F and Stroeve P 1996 *Chem. Mater.* **8** 2209

Kolen'ko Y V, Churagulov B R, Kunst M, Mazerolles L and Colbeau-Justin C 2004 *Appl. Catal. A: Environ.* **54** 51

Komarneni S, Fregeau E, Breval E and Roy R 1988 *J. Am. Ceram. Soc.* **71** C-26

Lagashetty A, Havanoor V, Basavaraja S, Balaji S D and Venkataraman A 2007 *Sci. Technol. Adv. Mater.* **8** 484

Li G S, Smith Jr R L, Inomata H and Arai K 2002 *Mater. Res. Bull.* **37** 949

Liu C, Zou B, Rondinone A J and Zhang Z J 2000 *J. Am. Chem. Soc.* **122** 6263

Lu J, Pascal J L and Favier F 1999 *Chem. Mater.* **11** 141

Maclaren I and Ponton C B 1998 *J. Mater. Sci.* **33** 17

Mallikarjuna N N, Govindraj B, Lagashetty A and Venkataraman A 2003 *J. Therm. Anal. Calor.* **71** 915

Matijevic E 1993 *Chem. Mater.* **5** 412

Matsumoto H 2003 *Physica* **B334** 112

McIntyre N S and Zetaruk D G 1977 *Anal. Chem.* **49** 1521

Niederberger M, Krumeich F, Hegetschweiler K and Nesper R 2002 *Chem. Mater.* **14** 78

Pal B and Sharon M 2000 *Thin Solid Films* **379** 83

Pawaskar N R, Sathaye S D, Bhadbhade M M and Patil K R 2002 *Mater. Res. Bull.* **37** 1539

Pileni M P and Moumen N 1996 *J. Phys Chem.* **100** 1867

Rao C N R 1963 *Chemical applications of infrared spectroscopy* (New York and London: Academic Press)

Siegal R W 1996 *Sci. Am.* **275** 74

Singh N K and Kushawaha S K 2000 *Transition Met. Chem.* **25** 648

Suresh K, Kumar N R S and Patil K C 1991 *Adv. Mater.* **3** 148

Titirici M -M, Antonietti M and Thomas A 2006 *Chem. Mater.* **18** 3808

Wen X, Wang S, Ding Y, Wang Z L and Yang S 2005 *J. Phys. Chem.* **B109** 215

White R L, New R M H, Fabian R and Pease W 1997 *IEEE Trans. Magn.* **33** 990

Yu H -F and Gadalla A M 1996 *J. Mater. Res.* **11** 663

Zheng Y, Cheng Y, Wang Y, Bao F, Zhou L, Wei X, Zhang Y and Zheng Q 2006 *J. Phys. Chem.* **B110** 3093